Testing of a Long-Burning-Time Paraffin-Based Hybrid Rocket Motor

Enrico Paccagnella,* Marco Santi,† Alessandro Ruffin,† Francesco Barato,‡ and Daniele Pavarin§
University of Padua, 35131 Padua, Italy
and
Gianluigi A. Misté,¶ Giovanni Venturelli,¶ and Nicolas Bellomo¶
Technology for Propulsion and Innovation, S.r.l., 35131 Padua, Italy

DOI: 10.2514/1.B37144

One of the main issues that prevents the widespread use of hybrid propulsion is the low regression rate of classical hybrid fuels. Recently, paraffin-based fuels have been proposed as a viable solution; however, concerns about paraffin thermomechanical properties have often been seen as a possible showstopper. A small-scale hybrid rocket, able to burn hydrogen peroxide and paraffin wax for an extended time, has been designed, built, and tested in order to investigate the suitability of paraffin wax as a hybrid fuel for actual missions. The motor has a nominal burning time of 80 s, which is compatible with the majority of the missions performed by rocket motors. The motor has been tested successfully, demonstrating that paraffin can be used on real missions. Two different types of paraffin were used: type A and type B, which have regression rates of 1.45 and 1.07 mm/s, respectively, at a reference oxidizer mass flux of 50 kg/m^2 · s and at a reference pressure of 15 bar. Moreover, temperature measurements inside the fuel grain demonstrated the liquid layer theory to be valid. An instrumented nozzle has also been used to better investigate the thermal behavior of the nozzle assembly.

Nomenclature

A_t	=	nozzle throat area
a, n	=	regression rate law coefficients
C_F	=	thrust coefficient
c^*	=	characteristic velocity
D	=	grain port diameter
G_{ox}	=	oxidizer mass flux
g_0	=	gravitational acceleration
Isp	=	specific impulse
L	=	grain length
$\dot{m}_f$	=	fuel mass flow
$\dot{m}_{ox}$	=	oxidant mass flow
O/F	=	mixture ratio
p_c	=	combustion chamber pressure
$\dot{r}$	=	regression rate
T	=	thrust
ρ	=	fuel density

I. Introduction

HYBRID rockets have long been recognized [1] as a propulsion option with strong potential due to their inherent advantages like simplicity, reliability, safety, start/stop/restart, and thrust control capabilities [2–4]. Unfortunately, to date, this potential has not been exploited [5–8]. One of the main reasons is related to the low regression rate of the fuel that is limited by the blocking mechanism of the convective heat transfer on the fuel surface caused by the blowing of the ablating fuel [9–11]. Even for moderate thrusts, this low regression rate prevents the realization of fuel grains with an acceptable volume loading and length [12]. Since the 1960s, for several decades, the main way to address this issue has been the use of multiport grains [13,14]. However, multiport grains are penalized by complexity (e.g., of casting, ignition, injection, etc.), structural issues, different mass flows/regression rates between ports, and high fuel residuals [15,16]. For this reason, a significant effort has been spent in recent years to find a way to increase the regression rate in order to use a much more effective single-port geometry [17]. Some interesting solutions investigated were the addition of energetic materials [18–21] or innovative injection patterns [22–27] and innovative devices [28]. One promising solution was the use of a new class of fuels, first proposed by Karabeyoglu et al. and called liquefying fuels, generally based on paraffin wax [29–33]. These fuels melt on the surface, creating a thin liquid layer with a very low viscosity. Thanks to the low viscosity, the shear stresses of the port flow are able to perturb the surface, generating small waves. Fuel droplets detach from the tip of the waves and are entrained by the gas flow. Adding another mass transfer mechanism to the conventional one, paraffin-based fuels are able to reach a regression rate several times higher than conventional ones, thus giving the possibility to design single-port hybrids for several applications [34–36].

Paraffin-based fuels have been often regarded with skepticism due to their low melting temperature and softening point. Because these material properties could represent a limitation for specific applications with extended temperature range for long periods, there is often a common misconception on paraffin hybrid rockets: the paraffin grain will soften and melt during a long burn. Although, according to Karabeyoglu's liquid layer theory, the heat transfer from the flame is able to melt only a very thin layer near the surface, whereas the rest of the grain should remain at room temperature unless it is heated from other paths. With proper motor thermal insulation, a paraffin grain should be able to withstand a long burn.

Based on this theory, the main objective of the investigation presented in this paper was to prove experimentally the capability of paraffin-based fuels to operate successfully for a long burn without major issues. To achieve this goal, a laboratory-scale hybrid motor using high-test peroxide (HTP)/paraffin with a nominal vacuum thrust of 1 kN has been designed, built, and tested up to 80 s. To the

Presented as Paper 2017-4829 at the AIAA 53rd AIAA/SAE/ASEE Joint Propulsion Conference, AIAA Propulsion and Energy Forum, Atlanta, GA, 10–12 July 2017; received 23 March 2018; revision received 24 October 2018; accepted for publication 20 November 2018; published online 31 December 2018.

*Ph.D. Student, Center of Studies and Activities for Space "G. Colombo"; enrico.paccagnella.1@phd.unipd.it.
†Ph.D. Student, Center of Studies and Activities for Space "G. Colombo."
‡Research Fellow, Center of Studies and Activities for Space "G. Colombo."
§Associate Professor, Department of Industrial Engineering, Center of Studies and Activities for Space "G. Colombo."
¶Ph.D., Technology for Propulsion and Innovation.

knowledge of the authors, this is the longest burn of a paraffin-based hybrid motor ever documented. Moreover, in order to demonstrate the liquid layer theory, the temperature of the fuel block has been monitored during the burn. Finally, the heat transfer from the combustion gases to the motor walls/nozzle has been investigated/addressed. In general, the test demonstrated directly the feasibility of a small HTP/paraffin motor with a considerable long burn. Considering that the thermal/erosion issues should be more significant at small scale, the test demonstrated indirectly the feasibility of the technology also for larger motors.

The paper is divided in two main parts. In the first part (Secs. II and III), the experimental setup is described together with the results of the 80 s burn test. In the second part (Secs. IV and V), the setup has been modified in order to further investigate the thermal behavior of the nozzle. A different type of paraffin wax has been used to increase the fuel-rich mixture ratio of the tests. Two different instrumented nozzle configurations have been designed and fire tested to get further insight on the thermal heat transfer in the nozzle region.

II. Experimental Setup

The experimental setup can be divided in two parts: the fluidic line needed to regulate the oxidizer mass flow, and the hybrid 1 kN motor. The fluidic line includes the pressurization system, the oxidizer tank, the oxidizer feeding line with the valves for the regulation of the oxidizer mass flow, and other auxiliary items. The hybrid motor is composed of the catalyst bed that decomposes the HTP, the combustion chamber filled with the fuel grain cartridge, and the nozzle. A more detailed description of these elements is given in the following.

A. Fluidic Line

As schematized in Fig. 1, the fluidic line components are, starting from upstream, a high-pressure nitrogen (N_2) tank; the pressure regulation block consisting of two pressure regulators (PR1 and PR2) serially connected; the hydrogen peroxide tank; a series of tubes and automated ball valves connected by double ferrule fittings; and a variable area cavitating venturi (VACV), which can be used to modify the mass flow required in a test.

Inside the hydrogen peroxide tank, two volumes are separated by a piston: the aforementioned volume hosts the pressurant, whereas the lower volume holds the oxidizer. The impermeability of the piston is granted by specific sealing. Connected to the piston and directed upward, there is a stem that crosses the uppermost bulkhead and is directly linked to a linear potentiometer. Thanks to the potentiometer signal output, both the instantaneous mass flow and cumulative mass can be determined. This is a good method to measure the mass flow over a wide range of values. Two HTP tanks are available for the experiments: one for short burns (4L capacity) and the other for longer burns (12L). To guarantee the accuracy of the measurements, before each test, most of the gas and fluid in the lower volume is vacuum removed before filling up, thus reducing the ullage volume during the fire tests.

There are three pressure sensors mounted on the fluidic line: p_{tank} is screwed in the upper bulkhead of the tank, and hence measures the pressurant pressure in the oxidizer tank; and p_{up} and p_{down} are placed, respectively, upstream and downstream of the cavitating venturi. A thermocouple, placed at the tank outlet, measures the outflow temperature in order to compensate for the density data and for safety reasons in case of eventual HTP dissociation inside the tank. Valves V_{05} and V_{tank} are manually actuated before tank loading and pressurization. V_c and V_{test} are electrovalves pneumatically actuated in this order during the tests. V_{purge} is pneumatically and remotely actuated; when opened, it allows low-pressure N_2 to flow through the last section of the line in order to purge this last volume from any residual HTP still present at the end of the burn. The downstream volume, between V_{test} and the engine catalytic injection, is kept to a minimum. V_{dump} is pneumatically and remotely actuated as well, but its function is to empty and depressurize the line volume between V_c and V_{test}.

To ensure full safety during the tests, various rupture disks and relief valves are mounted at different places of the tank and the fluidic line; in case of overpressure, the high-pressure gases are vented to the atmosphere outside of the testing area.

B. Hybrid Motor

The hybrid motor is composed of a catalytic reactor (or the catalyst bed) and the combustion chamber. The catalytic function is to decompose the 90% HTP with an exothermic reaction, producing a high amount of heat. The reaction products of oxygen and water are then injected directly in gaseous form inside the combustion chamber at a temperature between 700 and 800°C; here, the hot oxygen will ignite the paraffin grain, starting the combustion process. The pressure inside the combustion chamber can be estimated by the usual equation:

$$p_c = \frac{(\dot{m}_{\text{ox}} + \dot{m}_f)c^*}{A_t} \tag{1}$$

In a hybrid motor, if the oxidizer mass flow is known, the fuel mass flow (assuming a cylindrical port consumption) can be predicted as follows:

$$\dot{m}_f = \rho \pi D L \dot{r} \tag{2}$$

where the space-averaged regression rate, for a paraffin fuel, is expected to follow the empirical law:

$$\dot{r} = a G_{\text{ox}}^n \tag{3}$$

It is easy to demonstrate that, if the exponent n in Eq. (3) is equal to 0.5, the mixture ratio is constant during the burn at any port diameter size. For a paraffin fuel with HTP or nitrous oxide, $n = 0.5$ is a good assumption, as was already demonstrated by several international

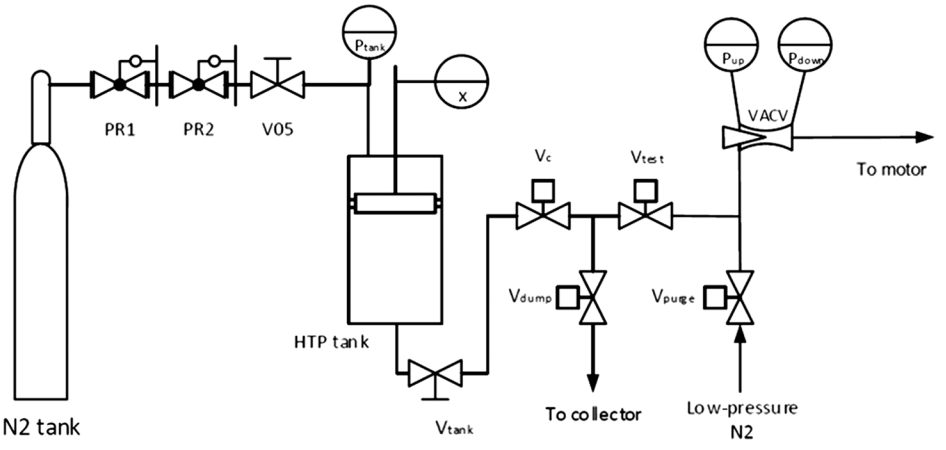

Fig. 1 Fluidic line and instrumentation.

researchers [37–39] and confirmed in our laboratory during other test campaigns performed under similar conditions. The mixture ratio, or O/F ratio, is defined as follows:

$$\mathrm{O/F} = \frac{\dot{m}_{\mathrm{ox}}}{\dot{m}_f} \tag{4}$$

The optimal O/F for HTP/paraffin hybrid motors, which is able to maximize the characteristic velocity c^* and the specific impulse Isp, is around 6.5–7.5. During the grain burn, the internal geometry of the motor changes due to the consumption of both the fuel grain and the thermal protections. However, if we assume that c^* is mainly affected by the O/F value and only slightly affected by this change in the fluid-dynamic flow pattern, between the start and end of the burn, we should expect an almost constant efficiency (i.e., constant c^*). Therefore, if the oxidizer mass flow is held constant, given all the aforementioned assumptions, it is reasonable to expect a constant chamber pressure in Eq. (1) if no erosion of the nozzle throat occurs (i.e., A_t is constant during the burn). This allows for an almost constant thrust during the entire burning time:

$$T = \dot{m}c^*C_F = \dot{m}\mathrm{Isp}g_0 \tag{5}$$

The objective of the present study is to determine the suitability of paraffin as a hybrid rocket fuel for long burning times. Because the main objective is to characterize the paraffin fuel behavior, no convergent–divergent nozzle is employed in the tests and the thrust measurement is not carried out. In fact, the combustion efficiency (i.e., the experimental c^*) can be estimated by directly measuring the chamber pressure using a convergent nozzle, as is clear from Eq. (1). More accurate studies will be made in the future to better assess the efficiency and thrust of the proposed motor configurations; these measurements are out of the scope of the present experimental campaign.

Hereafter, the design and the configuration of the hybrid motor used in the tests are described. The combustion chamber, visible in Fig. 2, is made of steel and is composed of a cylinder and two flanges, which are linked to the cylinder with two pairs of clamps. This type of connection permits a quick assembly/disassembly procedure, allowing for an increase in the number of tests per day. In addition, a high-temperature graphite gasket is employed to ensure proper sealing of the different components. The first flange is directly linked to the catalyst bed, whereas the second flange is designed to enclose a graphite nozzle that is held in place by a steel cap (see Fig. 3 for a clearer view). The nozzle employed in the experimental tests is only convergent, for the reasons exposed previously. The combustion chamber elements are all designed to withstand a maximum expected operating pressure of 40 bar with a safety factor of four, with the exception of the nozzle cap bolts, which are designed to fail in case of a pressure higher than 60 bar. This choice has been made in order to prevent damage to the motor and the experimental setup in the occurrence of an unexpected overpressure event inside the combustion chamber.

The combustion chamber presents 22 sensor holes for installing thermocouples, pressure sensors, or other instrumentation devices in order to take accurate measurements inside the chamber during the burn. In particular, the thermocouples cannot be used to monitor the chamber interior temperature because of the too high temperature of the burned gases; however, if placed inside the paraffin grain at different radii, they can be used as a means to measure the regression rate, as will be demonstrated in later sections.

Inside the combustion chamber, the layout (visible in Fig. 3) features a prechamber, the paraffin grain, and the postchamber. Both the pre- and postchambers need appropriate thermal protections to prevent the fire from touching the external metal casing. The material employed for the protections is high-density polyethylene (HDPE), which is able to insulate the casing by means of ablative cooling, having a regression rate much lower than paraffin wax but with the same specific impulse.

The testbench has been designed with two linear guides so that the hybrid motor is mounted on the slide units and can transmit its thrust to the block installed in the rear part of the bench. The structure

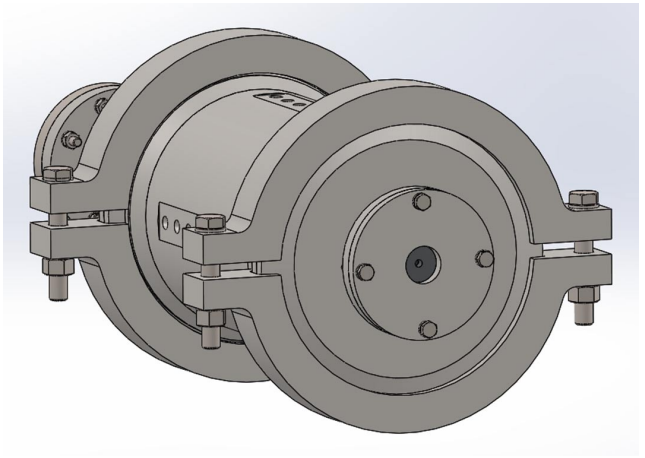

Fig. 2 Hybrid motor external casing.

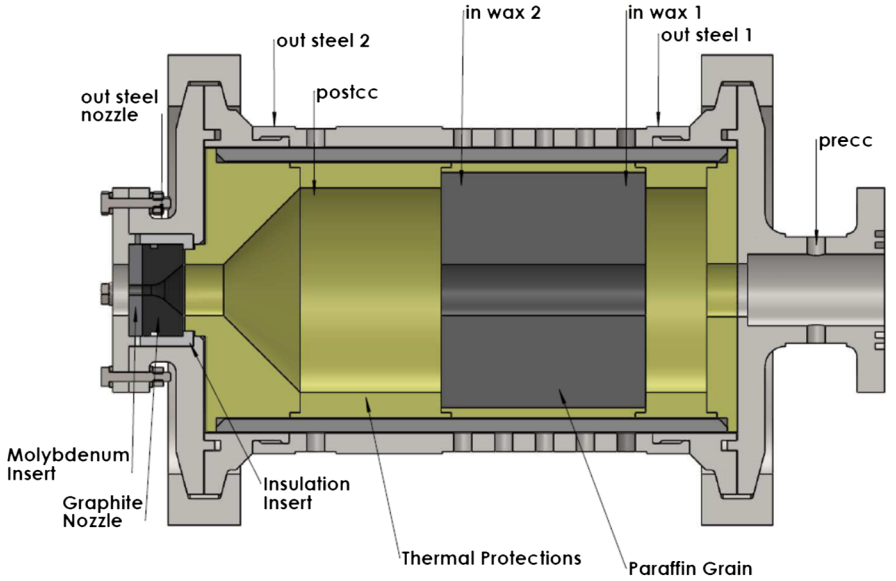

Fig. 3 Hybrid motor configuration for the long-burn test (80 s): on the upper side, the sensor positions; and on the lower side, the key motor elements definition.

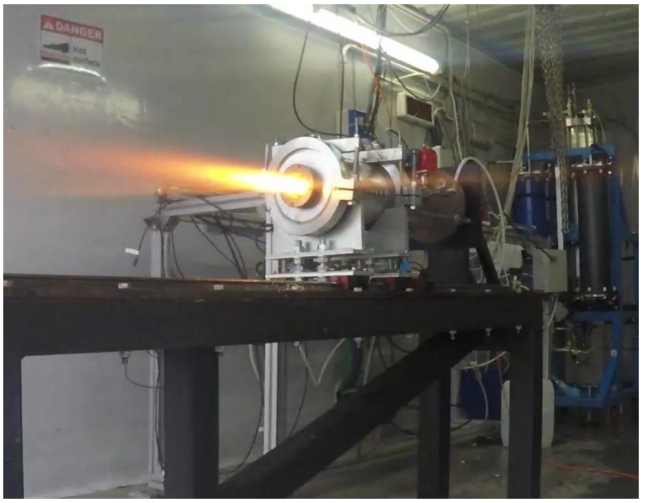

Fig. 4 Fire test. Note the experimental setup: two HTP tanks in the back, the test bench with its rear block, and the hybrid motor.

between the block and the motor allows for the installation of a load cell capable of measuring the motor thrust. The complete experimental apparatus is visible during a fire test in Fig. 4.

III. Long-Burn Eighty-Second Test

As stated in the Introduction (Sec. I), the objective of the long burn was twofold: first, to demonstrate the feasibility of the HTP/paraffin hybrid motor for long burning times; and second, to demonstrate paraffin liquid layer behavior. To achieve these goals, a specific motor setup has been implemented. This setup was designed in order to properly survive the severe thermal loads of such prolonged combustion and to allow the measurement of the temperature in the paraffin grain at different locations during the burning time. A detailed description of this setup is given in the following.

A. Motor Configuration and Sensor Setup

A long-burn test necessitates a complete insulation to avoid thermal damages to the external metal casing. For this reason, a double HDPE protection, visible in Fig. 3, is employed. The pre- and postchamber protections (in yellow in Fig. 3) are sealed with the grain casing with high-temperature silicone; these internal protections are then inserted in an external casing (in gray), and the whole assembly is sealed with the front and back protections (in yellow). This thermal protection layout consists of a practical cartridge that can be inserted and taken out from the metal casing quickly.

The hot oxidant flow enters the chamber from the inlet flange, coming from the right, and impinges on the grain surface, igniting the paraffin grain. The thermal protections also take part in the combustion process, providing the necessary ablative cooling capability, which prevents the metal casing from overheating. There are mainly two heat paths to the metal casing: the first is through the inlet catalytic flange, in which the metal sees a temperature of about 700–800°C; the second is through the nozzle, and it is more dangerous, not only because the flow temperature is far beyond 2000°C but also because the maximum heat transfer from the flow to the walls occurs at the nozzle throat, as is well known from gas dynamics. For this reason, the possibility of introducing an insulating material between the graphite nozzle and the metal casing is taken into consideration in the design phase. However, a good insulation tends to increase the graphite nozzle operating temperature, thus leading to an increase of the nozzle throat erosion phenomena typically occurring in long-burning-time tests. This in turn will translate into a decreasing, instead of constant, pressure profile. It is therefore decided to give prior importance, in this test, to stable pressure conditions: instead of using an insulating material, a steel insert is used in direct contact with the graphite nozzle. In addition, because graphite erosion is well known, especially in oxidant ambient, a molybdenum insert is employed in order to reduce the throat area change to a minimum. For the combustion temperature given by the reaction of HTP and paraffin wax (between 2000 and 2500°C, depending on O/F), the molybdenum seems a possible interesting solution; in fact, NASA experiments performed on solid rocket motors by Johnston et al. [40] confirmed that molybdenum was able to withstand a low-oxidizing flame temperature above 3000°C for nearly 30 s, with negligible erosion.

On the upper side of Fig. 3, the sensor positions employed for temperature and pressure measurements are marked. The flow pressure is measured before entering the combustion chamber (precc) using an extensimetric pressure transducer (gauge, 100 bar full scale, 0.25% accuracy, 1 ms response time, and 2000 Hz maximum frequency response) and in the back side of the chamber near the nozzle (postcc) using a piezoresistive pressure transducer (absolute, 70 bar full scale, 0.1% accuracy, less than 1 ms response time, and 2000 Hz maximum frequency response). Between the pressure sensor in the combustion chamber and the motor interface, a short tube filled with water is placed in order to protect it from the high temperature of the flow; postprocessing Fast Fourier Transform of the signal is done to prove that, according to the theory, no components of the signal are filtered by the liquid medium as compared to a tube filled with air [41]. The outside casing temperature is measured at the beginning and the end of the combustion chamber (out steel 1-2), but the most interesting temperature to be monitored is in the nozzle neck on the output flange (out steel nozzle), which has to be carefully monitored because no insulation of the graphite nozzle is employed. Two additional thermocouples are inserted inside the paraffin grain, at a depth of 10 mm from the grain external diameter; their duty is to monitor eventual temperature variations inside the grain during the burn. All the thermocouples employed are J types (±2.2°C accuracy), which are characterized by a temperature limit of about 750°C. The motor tests are controlled using a custom Programmable Logic Controller control and data acquisition system with a sampling frequency of 1 kHz for the pressure sensor and 10 Hz for the thermocouples.

The motor is designed to operate at a nominal mass flow of 300 g/s; however, the mass flow is reduced to 53 g/s in order to have the possibility of testing the long-burn capabilities of HTP/paraffin motors at a small scale. In fact, in the case of the test with the proprietary formulation type-A paraffin that has a higher regression rate, a higher mass flow would increase the consumption of the fuel too much, leading to a full grain consumption well before the end of the test. Moreover, a reduced oxidizer mass flow is able to decrease the erosion rate of the nozzle, which will help to maintain a constant value of the combustion chamber pressure. The data related to the testing conditions are exposed in Table 1.

B. Test Results

The long-burn test was completed successfully: no particular issues nor combustion instabilities were reported. First of all, the HTP mass flow measured by the potentiometer is reported in Fig. 5: the use of the cavitating venturi ensured an approximately constant oxidizer mass flow (the small waves were related to the process of filtering the noise of the potentiometer measurement).

The most important performance parameter for the test is the chamber pressure shown in Fig. 6: the constant trend of the plot of both precc and postcc pressures demonstrates that the HTP/paraffin hybrid motor is suitable to be used for long burning times, eliminating any doubt related to the use of a paraffin grain for typical applications.

Table 1 Testing conditions for the long-burn test (80 s)

Parameter	Value
Paraffin wax	Type A
Grain length	100 mm
Grain external diameter	115 mm
Initial port size	20 mm
Burning time	80 s
HTP mass flow	53 g/s
Initial G_{ox}	168.7 kg/(m^2 · s)
Throat initial diameter	10 mm

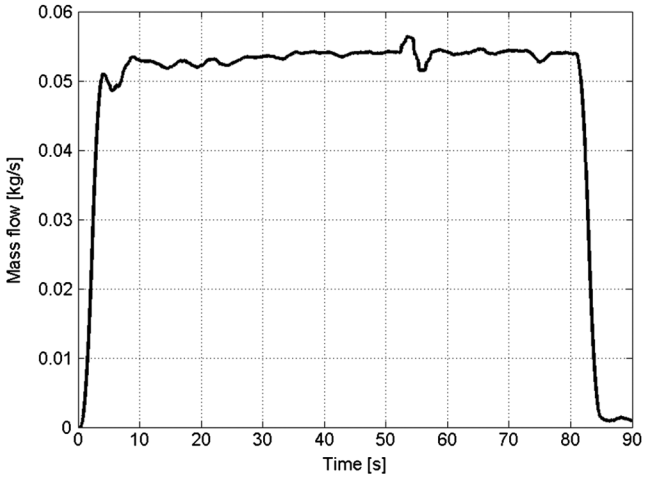

Fig. 5 HTP mass flow for the long-burn test (80 s).

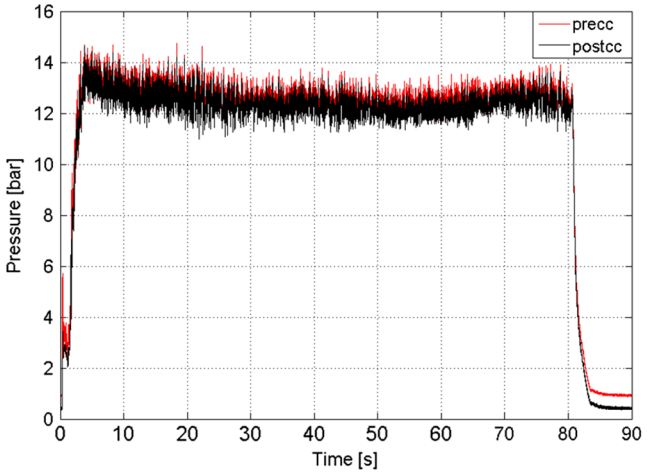

Fig. 6 Upstream (precc) and downstream (postcc) pressures measured in the combustion chamber during the long-burn test (80 s).

Moreover, the pressure oscillations, which can be reduced with a combustion chamber design optimization, are currently less than 10%, providing a stable and efficient combustion. Two other conclusions can be derived from Fig. 6. First, the use of the molybdenum insert prevents the erosion of the nozzle throat: in fact, the throat diameter measured at the end of the burn confirms the pressure data; the remaining graphite part of the nozzle, instead undergoes remarkable erosion. Second, assuming a constant value for c^* during the burn, because the oxidizer mass flow is held constant, the experiment confirms that the regression rate exponent n is equal to 0.5 for this type-A paraffin, as already anticipated in Sec. II; this also leads to the conclusion that the O/F ratio along the entire burning time remains unchanged.

At the end of the burn, only a little paraffin residual is found; the final weight measurements of the residuals are taken in order to determine the paraffin regression rate. Subsequent postprocessing also leads to the derivation of the regression rate constant value, which is found to be $a = 0.145\ (\mathrm{mm/s})(\mathrm{m}^2 \cdot \mathrm{s/kg})^{0.5}$.

Figure 7 shows the temperature variation with time of different points of interest. At the location in wax 1-2, both the thermocouples that were positioned 10 mm inside the grain measure an almost constant temperature (same as initial) until a steep increase is detected around 55 s: the sensors are exposed directly to the flame, and failure of the thermocouples (which is expected) occurs. At out steel 1-2, both the thermocouples experience a negligible temperature variation; a sign that the external case is well insulated from the flame zone. At out steel nozzle, the absence of any type of insulation around the graphite and molybdenum parts of the nozzle leads to a continuous increment of

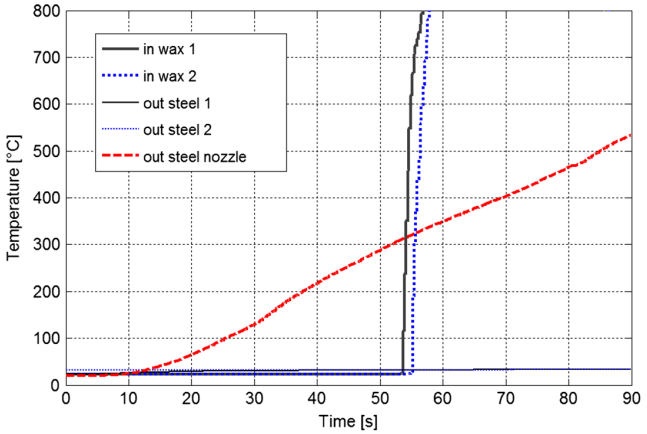

Fig. 7 Temperature measured in key station points during the long-burn test (80 s).

the temperature at this point, which is constantly monitored and reaches 500°C during the burn. At this temperature, the yield stress of the steel material becomes approximately half that of the ambient temperature, but thanks to the battleship design of the chamber, which employed a high safety factor, there is no risk of damaging the structure.

It is interesting to notice that Fig. 7 also represents an important validation of the regression rate relationship [Eq. (2)]. In fact, if we plot the curve of the theoretical port diameter vs time using the a, n regression rate constants (Fig. 8), at 55 s, we obtain a diameter value near 95 mm (approximately equivalent to the thermocouple depth of 10 mm): a value that is experimentally confirmed by the thermocouple exposure to the direct flame. Moreover, Fig. 7 shows another important point for a paraffin hybrid motor, namely, that the paraffin liquid layer blocks the heat penetration inside the grain during the burn, preventing the entire grain from being melted by a temperature increase.

The theoretical regression rate variation with time is plotted in Fig. 9: it is evident that paraffin achieves a considerable regression rate even at low G_{ox} with respect to other hybrid rocket fuels. Also, a relevant amount of HDPE mass, ablated from the thermal protections, is consumed during the burn. The burned HDPE mass accounts for approximately one-third of the total burned mass, bringing the global O/F value down to 3.3 (i.e., fuel-rich conditions), which is far from the optimal value (6.5–7.5, corresponding to maximum c^* and Isp); the implementation for future tests of more sophisticated thermal protections based on phenolic materials is ongoing. Even if it is not one of the goals of the present study, the average motor efficiency (calculated by comparing the theoretical c^* calculated with a thermochemical code [42] and the measured value at the same O/F) is found to be around 93%, which is a very good value for a preliminary configuration. However, this is expected because the motor is too

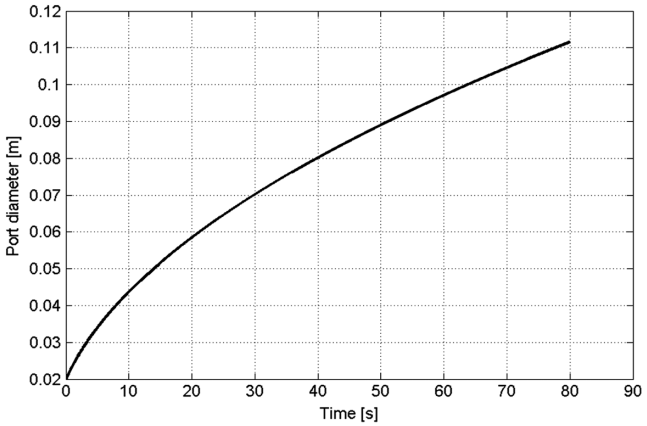

Fig. 8 Theoretical paraffin grain port diameter calculated with $a = 0.145$ and $n = 0.5$.

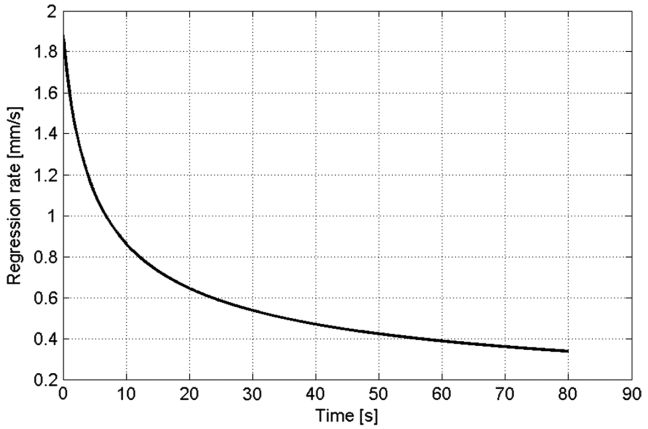

Fig. 9 Theoretical paraffin grain regression rate calculated with $a = 0.145$ and $n = 0.5$.

long for the low-oxidizer mass flow employed in the test: the combustion reagents have enough space to mix, and thus achieve an efficient combustion.

In conclusion, this test demonstrated that paraffin could be safely and effectively employed for even long-burn applications.

IV. Thermal Characterization Tests: Configuration One

A. Motor Configuration and Sensor Setup

The same internal motor configuration as for the long-burn test is employed (Fig. 3), but the outlet flange design has been changed in order to be able to install six thermocouples. These temperature measurements will help to define the thermal characterization of the nozzle region, monitoring the thermal gradients inside the different components. In configuration 1, just as in the long-burn test, no insulating material is used around the nozzle, but the usual steel insert is employed (as specified in Fig. 10).

Figure 10 shows the locations of the sensors: thermocouples T1 and T2 are inserted in the flat part of the steel flange; T3 monitors the temperature of the thermal protection and eventual hot gas leaks; T4 is attached to the steel adapter; T5 touches the graphite nozzle; T6 monitors the outside steel neck around the nozzle. It is possible to insert the thermocouples by drilling holes in the different elements and providing a sealing wherever necessary.

Another difference with the previous test is the paraffin chosen for the grain: the proprietary formulation type-B paraffin has a longer hydrocarbon chain composition, which leads to a higher melting point, a higher viscosity, and a lower regression rate; instead, the difference in the characteristic velocity is negligible, as can be seen from the plot in Fig. 11. Thanks to this characteristic, it is possible to increase the oxidizer mass flow up to 72 g/s without completely depleting the fuel in case of an 80 s burn.

Four tests have been carried out using this configuration: each with a different burning time (i.e., 10, 20, 60, and 80 s) in order to determine the repeatability of the thermal data. Table 2 summarizes the initial test conditions for configuration 1.

B. Test Results

The four tests were completed successfully and no particular issues were reported. However, with respect to the first test (namely, the long-burn 80 s test with type-A paraffin), the pressure oscillations were more severe in the transient ignition phase, even if they were damped in a few seconds. This was related to a noisier catalyst bed performance due to its poisoning and wearing out after the long-burn test, and it was not caused by paraffin combustion; this was proved also by the pressure behavior of the monopropellant test performed before each firing, which showed the same oscillations. Moreover, the nozzle erosion played an important role in defining the pressure plots, which are visible in Fig. 12. The higher mass flow and O/F used in these tests led to increased oxidizing conditions at the nozzle throat, determining its consumption. Up to 40 s, the erosion was

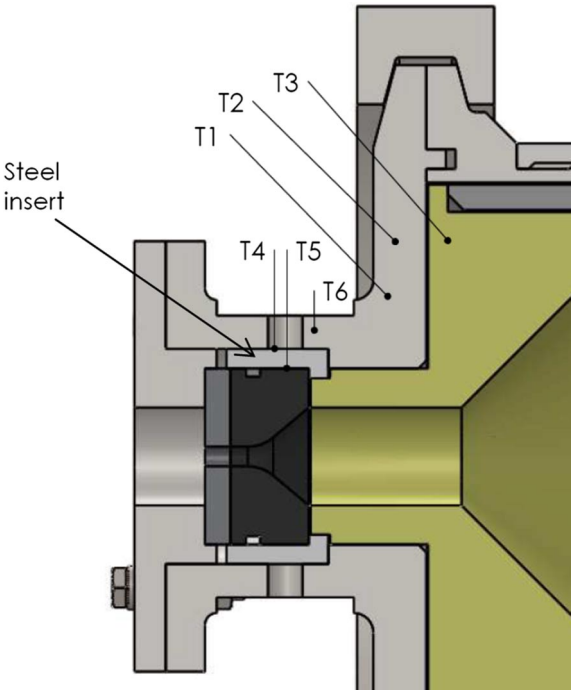

Fig. 10 Position of the thermocouples for the thermal characterization tests: configuration 1.

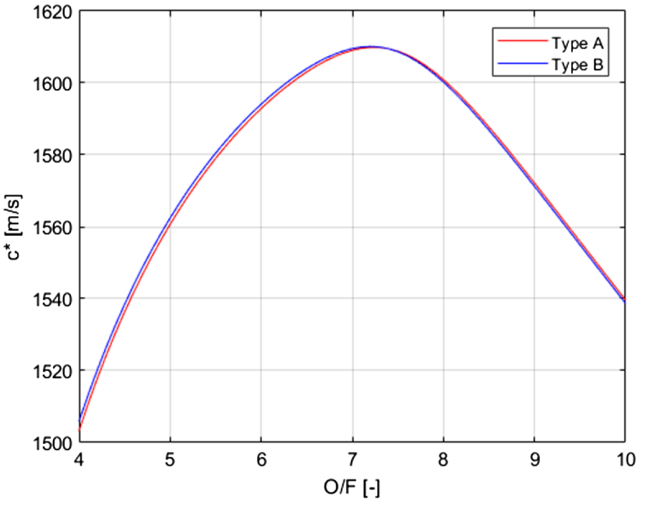

Fig. 11 Theoretical characteristic velocity as a function of mixture ratio for two different paraffin waxes with 91% hydrogen peroxide.

apparently negligible; then, there was an almost constant erosion rate with time: in fact, the nozzle throat diameters measured at the ends of the 60 and 80 s tests were, respectively, 11 and 12 mm. The throat diameter measurements were made before and after the test in order to

Table 2 Thermal characterization tests conditions: configuration 1

Parameter	Value
Paraffin wax	Type B
Insulation insert	Steel
Grain length	100 mm
Grain external diameter	115 mm
Initial port size	20 mm
Burning time	10, 20, 60, 80 s
HTP mass flow	72 g/s
Initial G_{ox}	229.1 kg/(m^2 · s)
Throat initial diameter	10 mm

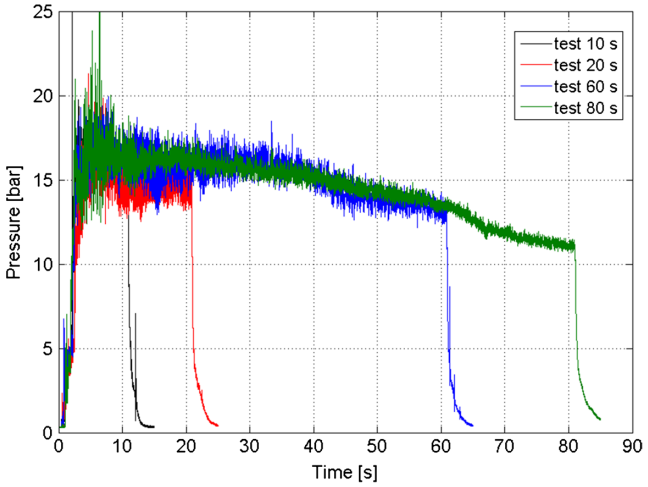

Fig. 12 Postcc pressure plot for different test cases.

investigate the relation to the pressure decays, which actually could also be originated by an O/F shift with time. For both the 60 s and the 80 s tests, the ratio between pre- and postburn throat areas and the ratio between initial and final chamber pressure values were compared: the two ratios were compatible to well within the ±5% experimental error. This meant that the pressure decay could be fully explained only by the throat erosion, and there was no evidence for a O/F shift; therefore, it was reasonable to assume $n = 0.5$ even with type-B paraffin. The same conclusion could also be drawn by measuring the paraffin mass burned in all the four tests: the burned mass measurements with different burning times had linear behaviors, and were thus all compatible with a constant paraffin mass flow. The final weight of the residuals has also been measured to determine the paraffin regression rate. Subsequent postprocessing led to the derivation of the regression rate constant value, which was found to be much lower with respect to the previous long-burn test: $a = 0.107\ (\mathrm{mm/s})(\mathrm{m}^2 \cdot \mathrm{s/kg})^{0.5}$. Corresponding to this value, a constant O/F ratio of 7.5 was found by considering only the paraffin fuel.

To estimate the motor overall efficiency, it is necessary to know the burned HDPE mass: in the four tests, it accounts on average for 40% of the total burned mass, bringing the global O/F value down to 4.5. This finding highlights the importance in the thermal protection choice and design: in fact, the paraffin O/F (7.5) is around the optimal value, whereas the global O/F (4.5) is considerably lower.

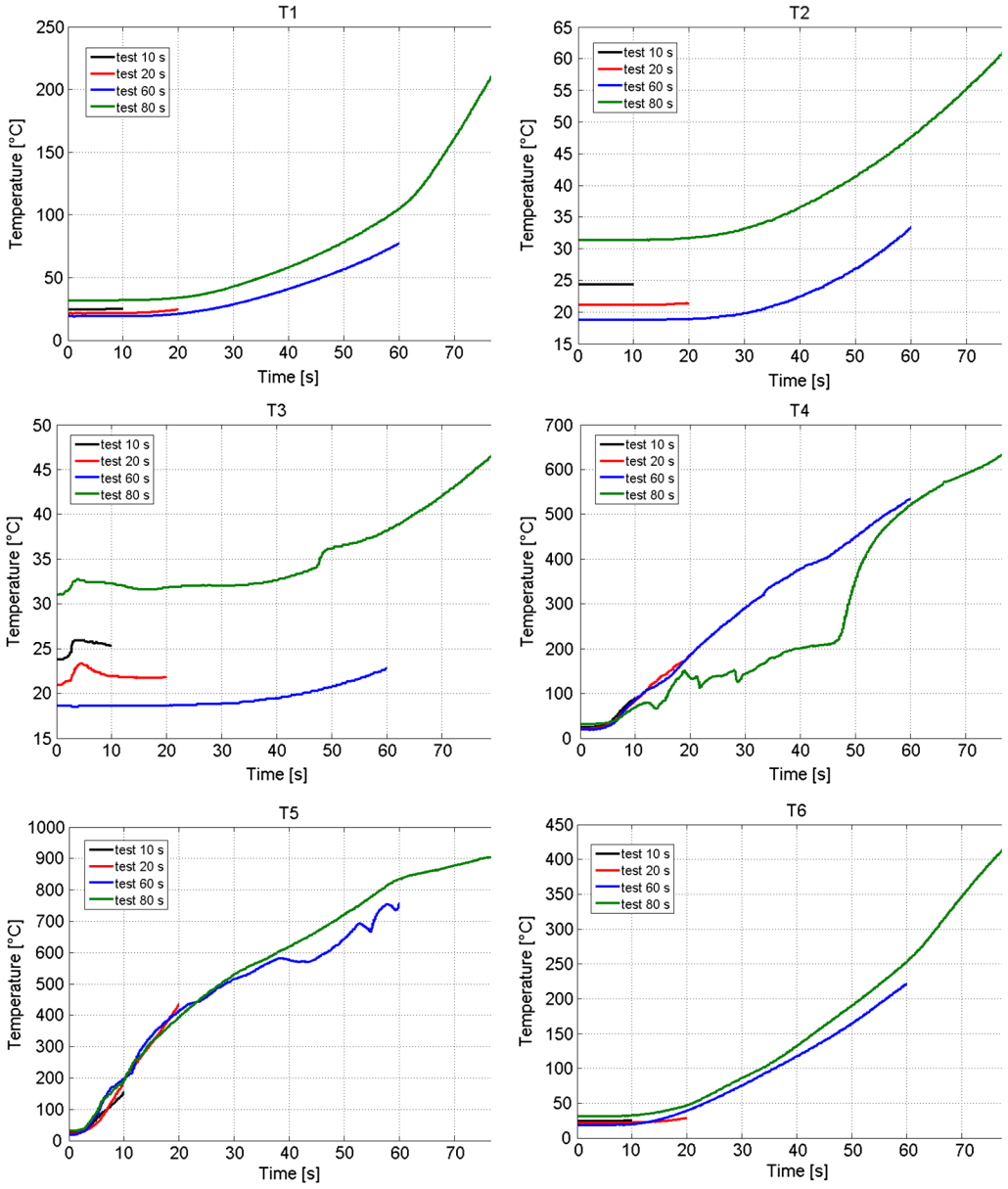

Fig. 13 Configuration 1: temperatures at different points of interest.

With respect to the first test (namely, the long-burn 80 s test with type-A paraffin), the lower regression rate of the paraffin and the higher oxidizer mass flow caused an increment of the global O/F from 3.3 to 4.5. The most notable effect given by this increase was the throat erosion. The mean motor efficiency corresponding to the aforementioned global O/F was around 94%.

Figure 13 summarizes the thermal data results obtained from the four tests of configuration 1. The following considerations can be drawn from the temperature vs time plots. The heat path started on the nozzle insert, which was the only part exposed to the combustion gases, and spread on the rest of the nozzle assembly. In fact, at any instant, the temperatures measured obeyed the following hierarchy (from maximum to minimum): T5, T4, T6, T1, T2, and T3. Referring to Fig. 10 for thermocouple locations, it is possible to asses that the flow is heating the graphite (T5) that, in turn, heats the surrounding metal (T4 and T6). Finally, the heat flow climbs the flange passing through point T1 up to point T2, finally transferring some heat also to the back of the thermal protections (point T3). It is worth noting that the temperature measurements demonstrate that the thermal protections are working efficiently: in fact, point T3 is not heated from the combustion flow but from the heat coming back from the nozzle throat region. In Fig. 12, the measurement on T4 for the 80 s test shows an anomalous behavior. The temperature rise is lower and more irregular than in the other cases. After 50 s, the temperature seems to recover the "nominal" trend. A nonperfect contact of the thermocouple with the metal could explain the lower heating and the erratic behavior due to thermal expansion and vibrations. After 50 s, eventually, the thermocouple gets back in better contact with the surrounding metal. The temperature rise in T2 and T3 is minimal. T1 reaches almost 250°C near the end of the longest burn. Instead, point T6 undergoes an almost double temperature increase. The steel insert interface (T4) is heated to almost 700°C. Finally, the graphite interface reaches 900°C, which means that the graphite interior is at much higher temperatures.

V. Thermal Characterization Tests: Configuration Two

A. Motor Configuration and Sensor Setup

Configuration 2, shown in Fig. 14, is almost equal to configuration 1 but with nozzle insulation. The insulating material chosen is a machinable compound of calcium silicate with a very low and stable thermal conductivity (0.27 W/(m·K), which is almost constant in the 200–700°C range). The insulating ring is placed around the graphite block.

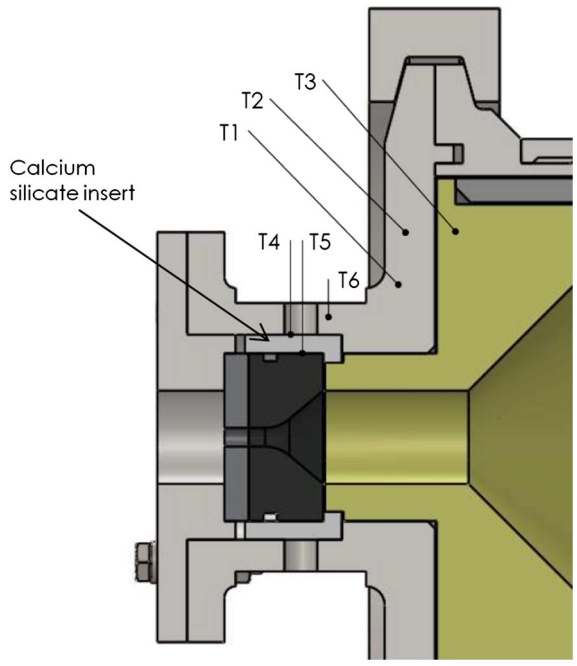

Fig. 14 Positions of the thermocouples for the thermal characterization tests: configuration 2.

Table 3 Thermal characterization tests conditions: configuration 2

Parameter	Value
Paraffin wax	Type B
Insulation insert	Calcium silicate
Grain length	100 mm
Grain external diameter	115 mm
Initial port size	20 mm
Burning time	10 s, 20 s, 40 s
HTP mass flow	72 g/s
Initial G_{ox}	229.1 kg/(m^2 · s)
Throat initial diameter	10 mm

Table 3 summarizes the initial test conditions for configuration 2: only 10, 20, and 40 s burning time cases were performed. The 40 s limit was chosen as an erosion limit given by the previous tests in order to obtain a still flat pressure profile.

B. Test Results

The three tests (i.e., 10, 20, and 40 s) were performed and completely successfully, and no particular issues were reported. The pressure oscillations were more severe in the 10 and 20 s tests, which were once again dependent on the noisy catalyst bed performance. The choice of a 40 s maximum burning time resulted in the absence of nozzle erosion, even if the calcium silicate insulation was employed: the result was a constant pressure profile for each of the three tests (Fig. 15).

The average values of the mixture ratio, the regression rate, and the efficiency are in line with the previous results obtained with configuration 1 (within the ±5% experimental error).

The most interesting differences to analyze in this case are related to the thermal field distribution. Figure 16 summarizes the thermal data results obtained from the tests of configuration 2. The temperature vs time plots, as in the previous case, show that the heat path starts on the nozzle insert, which is the only part exposed to the combustion gases, and spreads onto the rest of the nozzle assembly. Again, at any instant, the temperatures measured obey the usual hierarchy (from maximum to minimum): T5, T4, T6, T1, T2, and T3. Even in this case, the plastic thermal protections are isolating the metal from the combustion gases. With respect to the previous tests, it is possible to assess that the calcium silicate insert is also efficiently working as an insulator. In fact, all the thermocouples placed after the ceramic insulator along the heat path measure an almost negligible temperature rise (T6, T1, T2, and T3). The calcium silicate keeps the majority of the heat on the graphite insert, which reaches much higher temperatures than with configuration 1 (T5). The calcium silicate

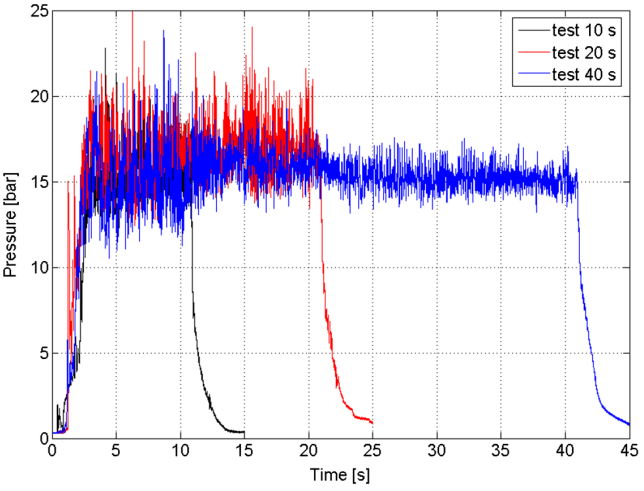

Fig. 15 Postcc pressure plot for different test cases.

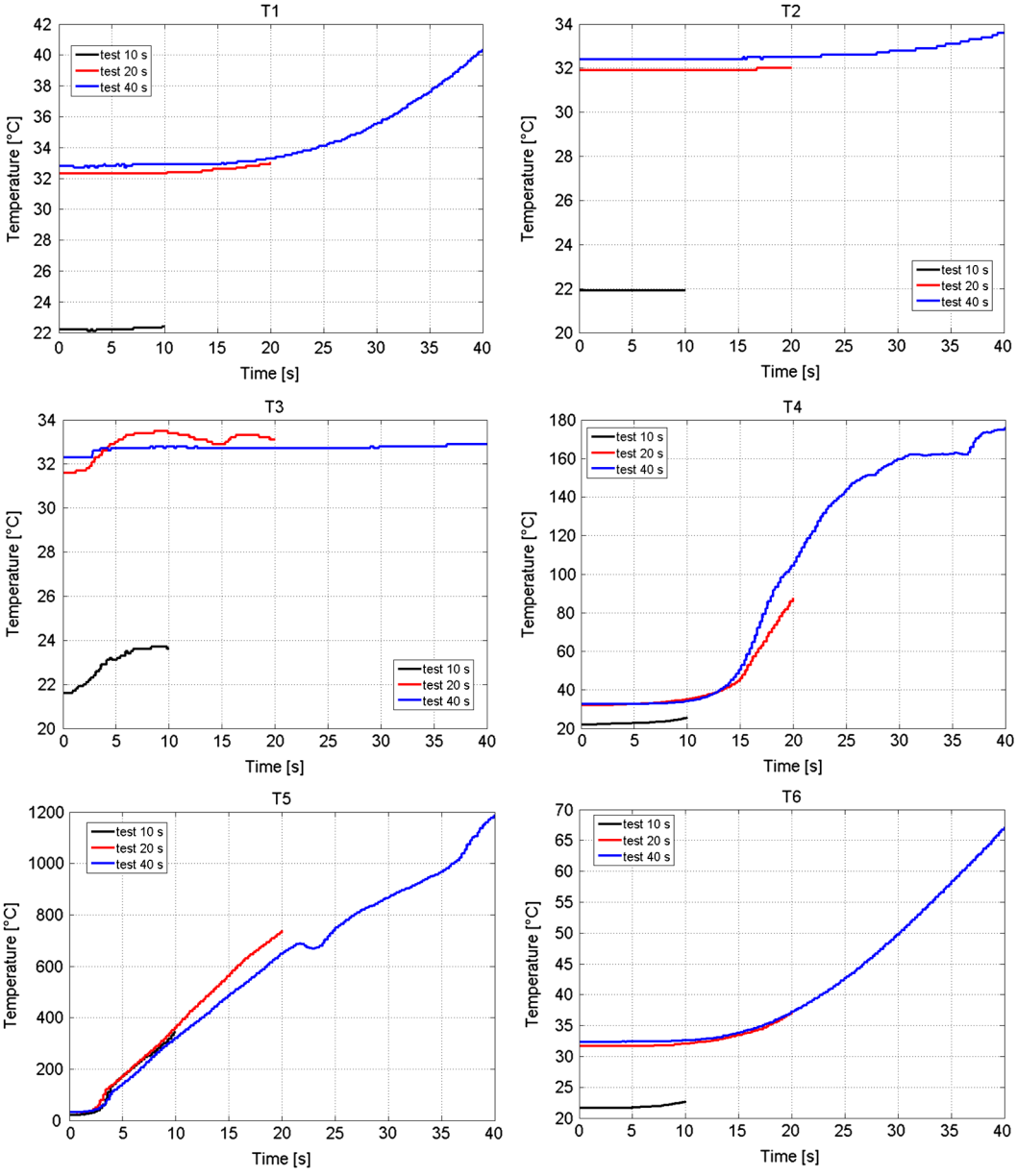

Fig. 16 Configuration 2: temperatures at different points of interest.

interface (T4) reaches nearly 180°C after 40 s, which is a much lower value than with the metal insert used in configuration 1.

From the point of view of protecting the external structural components of the motors from overheating, the ceramic insulation is very effective. However, the faster heating rate of the nozzle throat could exacerbate the issue of nozzle erosion.

To develop a flight-weight nozzle is important when carrying out a proper tradeoff between limiting the heat soakback to the combustion chamber case without compromising the throat integrity. A possible compromise for high-expansion-ratio space nozzles is to insulate the nozzle in the direction of the combustion chamber and define a heat path toward the nozzle extension in order to exploit radiative cooling.

VI. Summary and Final Considerations

Eight different tests have been performed in order to investigate the suitability of paraffin wax as a hybrid fuel for actual missions and to better investigate the thermal behavior of the nozzle assembly. A complete test matrix together with the main experimental results is presented in Table 4.

Table 4 Test matrix and summary of main experimental results

Test	Purpose	Paraffin wax	Insulation insert	HTP mass flow, g/s	Burning time, s	Efficiency, %
1	Long burn	Type A	Steel	53	80	93.1
2	Thermal characterization	Type B	Steel	72	10	94.9
3	Thermal characterization	Type B	Steel	72	20	93.5
4	Thermal characterization	Type B	Steel	72	60	94.7
5	Thermal characterization	Type B	Steel	72	80	94.3
6	Thermal characterization	Type B	Calcium silicate	72	10	94.3
7	Thermal characterization	Type B	Calcium silicate	72	20	93.6
8	Thermal characterization	Type B	Calcium silicate	72	40	95.2

Unfortunately, it proved to be quite difficult to make a comparison between the experimental results of this test campaign (in particular, the regression rate) and the data that can be found in literature. This is mainly due to the lack of reported experiments using the combination of HTP/paraffin as propellant: a similar approach to the one described in this paper was adopted in Ref. [43], for which the results were somewhat questionable because of the really high value of n obtained (around 0.96), which was even higher than the one predicted by Marxman's classical theory [10].

Most of the laboratory-scale experiments of hybrid rocket motors with paraffin that are presented in the literature use gaseous oxygen or nitrous oxide, making it impossible to directly compare these results with the ones presented in this paper. Nevertheless, they can be useful to get an impression of how the performance of this laboratory-scale motor correlates to similar approaches: obviously, the regression rate with gaseous oxygen is higher. In fact, the regression rate coefficients for this oxidizer are $a = 0.091$ and $n = 0.69$ in Ref. [44] and $a = 0.117$ and $n = 0.62$ in Ref. [45] (i.e., the regression rate is in millimeters per second, and the oxidizer mass flux is in kilograms per squared meter per second); whereas with nitrous oxide, the results are closer to the ones obtained with HTP, giving similar regression rate coefficients of $a = 0.178$ and $n = 0.5$ in Ref. [37], $a = 0.155$ and $n = 0.5$ in Ref. [38], $a = 0.184$ and $n = 0.5$ in Ref. [41], and $a = 0.171$ and $n = 0.5$ in Ref. [46] (i.e., the regression rate is in millimeters per second, and the oxidizer mass flux is in kilograms per squared meter per second).

VII. Conclusions

In recent years, there has been a renewed interest toward hybrid propulsion because of its positive features like simplicity, safety, affordability, reliability, environmental friendliness, and throttleability. Unfortunately, to date, the low regression rate of classical polymeric fuels has represented a showstopper for this technology. The introduction of paraffin-based fuels, which have shown regression rates several times higher, could finally unleash the potential of hybrid propulsion. However, concerns about paraffin thermomechanical properties have been raised by the propulsion community. Some of these concerns are exaggerated and/or based on an erroneous understanding of paraffin-based fuel physics/behavior.

The presented experimental study thus focused mainly on two main objectives: first, to demonstrate the feasibility of a high-test peroxide (HTP)/paraffin hybrid motor with a long burning time; and second, to demonstrate paraffin liquid layer theory, i.e., heat does not penetrate inside the fuel grain during the burn.

To achieve these goals, a HTP/paraffin laboratory-scale motor has been designed, built, and tested. The motor successfully burned for 80 s in fuel-rich conditions. The pressure profile was stable and constant, showing no sign of grain failure or degradation. The flat pressure profile without nozzle erosion also suggested a regression rate exponent near 0.5.

Two thermocouples were inserted in the fuel grain. They remained near room temperature until they were exposed to the port flow. The experiment thus demonstrated the validity of the liquid layer theory.

Another objective of the research was to investigate the thermal issues related especially to the nozzle, like throat erosion and heat transfer to the rest of the assembly. Two nozzles equipped with several thermocouples at different positions have been designed, built, and fire tested. The first one used a steel case around a graphite nozzle with a molybdenum insert. The second nozzle used a calcium silicate insulation around the graphite. The nozzles were tested with a paraffin wax with a higher carbon number (i.e., higher melting temperature) that provided a lower regression rate, and therefore a higher mixture ratio. The higher mixture ratio caused a slight erosion of the throat for long burns. The first nozzle was shown to be able to sustain the fire with relatively acceptable heating of the steel, whereas the graphite reached 900°C. The second nozzle showed a much higher heating of the graphite caused by the lower heat dissipation, keeping the rest of the system to much lower temperatures than the previous case.

The experimental results presented in this paper proved the validity of the liquid layer theory, which confirmed the possibility of using paraffin wax for a reasonable long burning time and encouraged the exploitation of this promising fuel for real applications.

Acknowledgments

The authors would like to acknowledge the effort and help in preparing and executing the tests that was given by the Propulsion Laboratory student team of 2016–2017: in particular, Alessio D'Ambros, Jacopo Di Geronimo, Igor Dorgnach, Alessandro Ferrari, Laura Lascialandà, and Luca Moro. Thanks go to Giorgio Massa and Roberto Torri from Solvay (Rosignano-Livorno, Italy) for the support and the procurement of the hydrogen peroxide.

References

[1] Ordahl, D. D., and Rains, W. A., "Recent Developments and Current Status of Hybrid Rocket Propulsion," *Journal of Spacecraft and Rockets*, Vol. 2, No. 6, 1965, pp. 923–926. doi:10.2514/3.28315

[2] Altman, D., and Holzman, A., "Overview and History of Hybrid Rocket Propulsion," *Fundamentals of Hybrid Rocket Combustion and Propulsion*, edited by M. J. Chiaverini, and K. K. Kuo, Vol. 218, Progress in Astronautics, and Aeronautics, AIAA, Reston, VA, 2007, pp. 1–36. doi:10.2514/5.9781600866876.0001.0036

[3] Altman, D., and Humble, R., "Hybrid Rocket Propulsion Systems," *Space Propulsion Analysis and Design*, Space Technology Series, edited by R. W. Humble, G. N. Henry, and W. J. Larson, McGraw–Hill, New York, 1995.

[4] Boardman, T., "Hybrid Propellant Rockets," *Rocket Propulsion Elements*, edited by G. P. Sutton, and O. Biblarz, Wiley-Interscience, New York, 2001.

[5] Grosse, M., "Design Challenges for a Cost Competitive Hybrid Rocket Booster," *2nd European Conference for Aerospace Sciences (EUCASS)*, EUCASS Paper 07–345, Brussels, July 2007.

[6] Kuo, K. K., and Chiaverini, M. J., "Challenges of Hybrid Rocket Propulsion in the 21st Century," *Fundamentals of Hybrid Rocket Combustion and Propulsion*, Vol. 218, Progress in Astronautics, and Aeronautics, edited by M. J. Chiaverini, and K. K. Kuo, AIAA, Reston, VA, 2007, pp. 593–638. doi:10.2514/5.9781600866876.0593.0638

[7] Karabeyoglu, A., "Challenges in the Development of Large-Scale Hybrid Rockets," *International Journal of Energetic Materials and Chemical Propulsion*, Vol. 16, No. 3, 2017, pp. 243–261. doi:10.1615/IntJEnergeticMaterialsChemProp.2018022732

[8] Barato, F., Bellomo, N., and Pavarin, D., "Integrated Approach for Hybrid Rocket Technology Development," *Acta Astronautica*, Vol. 128, Nov.–Dec. 2016, pp. 257–261. doi:10.1016/j.actaastro.2016.07.023

[9] Marxman, G. A., "Combustion in the Turbulent Boundary Layer on a Vaporizing Surface," *Symposium (International) on Combustion*, Vol. 10, No. 1, 1965, pp. 1337–1349. doi:10.1016/S0082-0784(65)80268-5

[10] Marxman, G. A., Wooldridge, C. E., and Muzzy, R. J., "Fundamentals of Hybrid Boundary-Layer Combustion," *Progress in Astronautics and Rocketry*, Vol. 15, Elsevier, 1964, pp. 485–522. doi:10.1016/B978-1-4832-2730-6.50025-7

[11] Chiaverini, M., "Review of Solid-Fuel Regression Rate Behavior in Classical and Nonclassical Hybrid Rocket Motors," *Fundamentals of Hybrid Rocket Combustion and Propulsion*, Vol. 218, Progress in Astronautics, and Aeronautics, edited by M. J. Chiaverini, and K. K. Kuo, AIAA, Reston, VA, 2007, pp. 37–126. doi:10.2514/5.9781600866876.0037.0126

[12] Pastrone, D., "Approaches to Low Fuel Regression Rate in Hybrid Rocket Engines," *International Journal of Aerospace Engineering*, Vol. 2012, 2012, pp. 1–12. doi:10.1155/2012/649753

[13] Story, G., "Large-Scale Hybrid Motor Testing," *Fundamentals of Hybrid Rocket Combustion and Propulsion*, Vol. 218, Progress in Astronautics, and Aeronautics, edited by M. J. Chiaverini, and K. K. Kuo, AIAA, Reston, VA, 2007, pp. 513–552. doi:10.2514/5.9781600866876.0513.0552

[14] Story, G., and Arves, J., "Flight Testing of Hybrid-Powered Vehicles," *Fundamentals of Hybrid Rocket Combustion and Propulsion*, Vol. 218, Progress in Astronautics, and Aeronautics, edited by M. J. Chiaverini,

and K. K. Kuo, AIAA, Reston, VA, 2007, pp. 553–592.
doi:10.2514/5.9781600866876.0553.0592

[15] Kearney, D. A., Joiner, K. F., Gnau, M. P., and Casemore, M. A., "Improvement to the Marketability of Hybrid Propulsion Technologies," *AIAA SPACE 2007 Conference and Exposition*, AIAA Paper 2007-6144, Sept. 2007.
doi:10.2514/6.2007-6144

[16] Barato, F., Grosse, M., and Bettella, A., "Hybrid Rocket Residuals—An Overlooked Topics," *50th AIAA/ASME/SAE/ASEE Joint Propulsion Conference and Exhibit*, AIAA Paper 2014-3753, July 2014.
doi:10.2514/6.2014-3753

[17] Casillas, E. D., Shaeffer, C. W., and Trowbridge, J. C., "Cost and Performance Payoffs Inherent in Increased Fuel Regression Rates," *33rd AIAA/SAE/ASME/ASEE Joint Propulsion Conference and Exhibit*, AIAA Paper 1997-3081, July 1997.
doi:10.2514/6.1997-3081

[18] Farbar, E., Louwers, J., and Kaya, T., "Investigation of Metallized and Nonmetallized Hydroxyl-Terminated Polybutadiene/Hydrogen Peroxide Hybrid Rockets," *Journal of Propulsion and Power*, Vol. 23, No. 2, 2007, pp. 476–486.
doi:10.2514/1.22091

[19] Risha, G. A., Evans, B. J., Boyer, E., and Kuo, K. K., "Metals, Energetic Additives, and Special Binders Used in Solid Fuels for Hybrid Rockets," *Fundamentals of Hybrid Rocket Combustion and Propulsion*, Vol. 218, Progress in Astronautics, and Aeronautics, edited by M. J. Chiaverini, and K. K. Kuo, AIAA, Reston, VA, 2007, pp. 413–456.
doi:10.2514/5.9781600866876.0413.0456

[20] Calabro, M., De Luca, L. T., Galfetti, L., Raina, H., and Perut, C., "Advanced Hybrid Solid Fuels," *Proceedings of the 58th International Astronautical Congress*, Paper IAC-07-C4.2.09, Hyderabad, India, Sept. 2007.

[21] Karabeyoglu, A., "Performance Additives for Hybrid Rockets," *Chemical Rocket Propulsion*, edited by L. T. De Luca, T. Shimada, V. P. Sinditskii, and M. Calabro, Springer Aerospace Technology, New York, 2016, pp. 139–163.
doi:10.1007/978-3-319-27748-6_5

[22] Majdalani, J., "Vortex Injection Hybrid Rockets," *Fundamentals of Hybrid Rocket Combustion and Propulsion*, Vol. 218, Progress in Astronautics and Aeronautics, edited by M. J. Chiaverini, and K. K. Kuo, AIAA, Reston, VA, 2007, pp. 247–276.
doi:10.2514/5.9781600866876.0247.0276

[23] Knuth, W. H., Chiaverini, M. J., Sauer, J. A., and Gramer, D. J., "Solid-Fuel Regression Rate Behavior of Vortex Hybrid Rocket Engines," *Journal of Propulsion and Power*, Vol. 18, No. 3, 2002, pp. 600–609.
doi:10.2514/2.5974

[24] Ronningen, J.-E., and Husdal, J., "Nammo Hybrid Rocket Propulsion TRL Improvement Program," *48th AIAA/ASME/SAE/ASEE Joint Propulsion Conference and Exhibit*, AIAA Paper 2012-4311, July–Aug. 2012.
doi:10.2514/6.2012-4311

[25] Barato, F., Faenza, M., Bellomo, N., Lazzarin, M., Bettella, A., and Pavarin, D., "Numerical Simulations of an H2O2 Vortex Hybrid Rocket Motor," *Space Propulsion*, Association Aéronautique et Astronautique de France (3AF), Bordeaux, France, May 2012.

[26] Bellomo, N., Barato, F., Faenza, M., Lazzarin, M., Bettella, A., and Pavarin, D., "Numerical and Experimental Investigation of Unidirectional Vortex Injection in Hybrid Rocket Engines Rockets," *Journal of Propulsion and Power*, Vol. 29, No. 5, 2013, pp. 1097–1113.
doi:10.2514/1.B34506

[27] Paccagnella, E., Barato, F., Pavarin, D., and Karabeyoglu, A., "Scaling Parameters of Swirling Oxidizer Injection in Hybrid Rocket Motors," *Journal of Propulsion and Power*, Vol. 33, No. 6, 2017, pp. 1378–1394.
doi:10.2514/1.B36241

[28] Bellomo, N., Lazzarin, M., Barato, F., Bettella, A., Pavarin, D., and Grosse, M., "Investigation of Effect of Diaphragms on the Efficiency of Hybrid Rockets," *Journal of Propulsion and Power*, Vol. 30, No. 1, 2014, pp. 175–185.
doi:10.2514/1.B34908

[29] Karabeyoglu, M. A., "Transient Combustion in Hybrid Rockets," Ph.D. Dissertation, Stanford Univ., Dept. of Aeronautics and Astronautics, Stanford, CA, 1998.

[30] Karabeyoglu, M. A., Altman, D., and Cantwell, B. J., "Combustion of Liquefying Hybrid Propellants: Part 1, General Theory," *Journal of Propulsion and Power*, Vol. 18, No. 3, 2002, pp. 610–620.
doi:10.2514/2.5975

[31] Karabeyoglu, M. A., and Cantwell, B. J., "Combustion of Liquefying Hybrid Propellants: Part 2, Stability of Liquid Films," *Journal of Propulsion and Power*, Vol. 18, No. 3, 2002, pp. 621–630.
doi:10.2514/2.5976

[32] Karabeyoglu, M. A., Cantwell, B. J., and Stevens, J., "Evaluation of Homologous Series of Normal-Alkanes as Hybrid Rocket Fuels," *41st AIAA/ASME/SAE/ASEE Joint Propulsion Conference and Exhibit*, AIAA Paper 2005-3908, 2005.
doi:10.2514/6.2005-3908

[33] Karabeyoglu, A., Zilliac, G., Cantwell, B. J., De Zilwa, S., and Castellucci, P., "Scale-Up Tests of High Regression Rate Paraffin-Based Hybrid Rocket Fuels," *Journal of Propulsion and Power*, Vol. 20, No. 6, 2004, pp. 1037–1045.
doi:10.2514/1.3340

[34] Karabeyoglu, A., Stevens, J., Geyzel, D., and Cantwell, B., "High Performance Hybrid Upper Stage Motor," *47th AIAA/ASME/SAE/ASEE Joint Propulsion Conference and Exhibit*, AIAA Paper 2011-6025, 2011.
doi:10.2514/6.2011-6025

[35] Karabeyoglu, A., "Advanced Hybrid Rockets for Future Space Launch," *5th European Conference for Aeronautics and Space Sciences (EUCASS)*, EUCASS, Munich, Germany, July 2013.

[36] Chandler, A. A., Cantwell, B. J., Hubbard, G. S., and Karabeyoglu, A., "Feasibility of a Single Port Hybrid Propulsion System for a Mars Ascent Vehicle," *Acta Astronautica*, Vol. 69, Nos. 11–12, 2011, pp. 1066–1072.
doi:10.1016/j.actaastro.2011.07.004

[37] Van Pelt, D., Hopkins, J., Skinner, M., Buchanan, A., Gulman, R., Chan, H., Karabeyoglu, M. A., and Cantwell, B., "Overview of a 4-Inch OD Paraffin-Based Hybrid Sounding Rocket Program," *40th AIAA/ASME/SAE/ASEE Joint Propulsion Conference and Exhibit*, AIAA Paper 2004-3822, 2004.
doi:10.2514/6.2004-3822

[38] McCormick, A., Hultgren, E., Lichtman, M., Smith, J., Sneed, R., and Azimi, S., "Design, Optimization, and Launch of a 3," Diameter N2O/Aluminized Paraffin Rocket," *41st AIAA/ASME/SAE/ASEE Joint Propulsion Conference and Exhibit*, AIAA Paper 2005-4095, 2005.
doi:10.2514/6.2005-4095

[39] Toson, E., and Karabeyoglu, A., "Design and Optimization of Hybrid Propulsion Systems for In-Space Application," *51st AIAA/ASME/SAE/ASEE Joint Propulsion Conference and Exhibit*, AIAA Paper 2015-3937, 2015.
doi:10.2514/6.2015-3937

[40] Johnston, J. R., Signorelli, R. A., and Freche, J. C., "Performance of Rocket Nozzle Materials with Several Solid Propellants," NASA Lewis Research Center, TN D-3428, Cleveland, OH, 1966.

[41] Bellomo, N., Barato, F., Faenza, M., Lazzarin, M., Bettella, A., and Pavarin, D., "Numerical and Experimental Investigation on Vortex Injection in Hybrid Rocket Motors," *47th AIAA/ASME/SAE/ASEE Joint Propulsion Conference and Exhibit*, AIAA Paper 2011-5675, 2011.
doi:10.2514/6.2011-5675

[42] Gordon, S., and McBride, J., "Computer Program for Calculation of Complex Chemical Equilibrium Compositions and Applications," NASA Lewis Research Center, Reference Publication 1311, Cleveland, OH, 1994.

[43] Brown, T. R., and Lydon, M. C., "Testing of Paraffin-Based Hybrid Rocket Fuel Using Hydrogen Peroxide Oxidizer," *Colorado Space Grant Consortium, AIAA Region 5 Student Conference*, Wichita, 2005.

[44] Karabeyoglu, M. A., Cantwell, B. J., and Altman, D., "Development and Testing of Paraffin-Based Hybrid Rocket Fuels," *37th Joint Propulsion Conference and Exhibit*, AIAA Paper 2001-4503, 2001.
doi:10.2514/6.2001-4503

[45] Karabeyoglu, A., Zilliac, G., Cantwell, B. J., DeZilwa, S., and Castellucci, P., "Scale-Up Tests of High Regression Rate Paraffin-Based Hybrid Rocket Fuels," *Journal of Propulsion and Power*, Vol. 20, No. 6, 2004, pp. 1037–1045.
doi:10.2514/1.3340

[46] Prendergast, L. M., Zimmerman, K. U., Silva, W. A., Chang, P. C., Sivaram, S., Kentosh, B. C., Chen, D. C., and Gambardella, A. L., "Paraffin Wax Based Experimental Hybrid Motor: Hybrid Propulsion Experiment," *UCLA Rocket Project—HyPE Paper*, UCLA Univ., 2010.

A. K. Gupta
Associate Editor